Progress In Electromagnetics Research Letters, Vol. 85, 125–130, 2019

Performance Evaluation of a Star-Shaped Patch Antenna on Polyimide Film under Various Bending Conditions for Wearable Applications

Fauziahanim C. Seman[1, *], Faisal Ramadhan[2], Nurul S. Ishak[1], Rudy Yuwono[2], Zuhairiah Z. Abidin[1], S. Haimi Dahlan[1], Shaharil M. Shah[1], and Adel Y. I. Ashyap[1]

Abstract—This paper proposes a prototype of a flexible antenna which utilizes a star patch design. The work seeks feasibility of the star patch antenna to maintain its characteristic when it is bending on a curvy structure. The patch antenna is fabricated on a 0.8 mm thickness, h of polyimide film with a dielectric constant, ε_r of 3.4. The simulation result in Computer Simulation Technology Microwave Studio (CST MWS®) software shows that the antenna provides a -10 dB bandwidth of 24.9% at 2.45 GHz with a minimum reflection coefficient, S_{11} of -26.67 dB in flat condition. The stability in its performance has been noticed in which the shift in the resonant frequency is less than 2% when the structure is bending on a curvy surface with a radius of 90 mm. The measured results in terms of reflection coefficient, bandwidth, radiation pattern, and gain demonstrate a good agreement with the simulated results.

1. INTRODUCTION

The main focus in modern technology is to have devices which not only are lighter and smaller in size, but also offer a great flexibility. In antenna design, the growth of wearable devices, which are not limited to on-body applications, increases the demand for the antenna to be fabricated on a flexible material. A number of flexible antennas have been realized on various flexible substrate materials such as textile [1, 2], paper [3], and thin film [4, 5]. Although it is suitable for wearable and conformal applications, fabric substrate is also prone to discontinuities, fluids absorption, and crumpling [6]. A tradeoff always exists between achieving functional conformability and low cost. As the wearable antenna will be used as a part of clothing which may follow the body curve, the structure deployed needs to be relatively insensitive to various bending conditions. In [7], a wearable dipole configuration is proposed for on-body applications. The antenna has been designed with a semi-flexible substrate, RO3003$^{\text{TM}}$, and its performance has been tested for different bending conditions that may be introduced by human body curvature.

In order to allow bending and need for flexibility, a robust yet compact antenna is typically designed based on microstrip approach [8]. Flexing the antenna from its nominal straight configuration can impact the performance, depending on the design, substrate material, and other factors. Consider a typical rectangular microstrip antenna where the width (W), length (L), thickness of the substrate (h), and dielectric constant (ε_r) are defined. If the antenna is bending along L, the performance degradation occurs due to the effective length, L_{eff}, variations when the new length, L, lies along an arc midway through the dielectric substrate, which therefore varies the effective width, W_{eff}, and length, L_{eff}, of

Received 21 February 2019, Accepted 14 May 2019, Scheduled 1 July 2019

* Corresponding author: Fauziahanim C. Seman (fauziahs@uthm.edu.my).

[1] Research Centre for Applied Electromagnetic, Universiti Tun Hussein Onn, Malaysia. [2] Telecommunication Laboratory, Department of Electrical and Electronic Engineering, Brawijaya University, Indonesia.

the patch and also the thickness of the dielectric substrate. Similar cases can be applied in bending the antenna along W. In reality, the resonant frequency and reflection coefficient of the antenna can be shifted or decreased depending on the bending environment, and the radiation pattern of the antenna can be distorted when the antenna is stretched, rolled on curvy surfaces, or twisted.

In this paper, a design consideration of the wearable antenna which utilizes the followings will be implemented; (i) a very thin substrate, (ii) a structure with a partial ground plane, (iii) a shape of antenna that is able to maintain the effective width and length during bending, and (iv) a feed line at the vertex of the curve. Therefore, a star patch antenna is chosen as it can compromise the bending effects. Kapton Polyimide film is used as the antenna substrate due to its good balance between the physical, chemical, and electrical properties with a low loss factor over a wide frequency range [8, 9].

2. ANTENNA GEOMETRY

The preliminary investigation on the star patch antenna started with a circular patch antenna, and the principal idea is motivated by the effectiveness of sharp edges to lengthen the surface current and therefore, is able to miniaturise size with a better gain [10, 11]. It can be observed from the empirical study that star-shape of the patch offers better antenna performance than circular shape in terms of the VSWR and reflection coefficient. The optimization of dimensions of the antenna is done by performing parametric studies. Figure 1 shows the geometry of the star patch antenna [10] which is fabricated on a 0.8 mm thickness, h, of polyimide film substrate with a dielectric permittivity, ε_r, of 3.4 and loss tangent, $\tan\delta$, of 0.002. The star patch is connected to a 50 Ω termination line feed. At the back of the structure, a partial ground plane is employed to produce an omnidirectional radiation pattern. In addition, the partial ground plane technique is also adopted for size reduction. Impact of the removal area is carefully observed during the design process, to ensure that a good impedance matching characteristic is obtained. The overall size of the proposed antenna is $75 \times 50\,\text{mm}^2$. The prototype is realized with an aluminum tape by using manual stencil. The manufacturing tolerance for the physical dimensions is found less than ± 0.5 mm. It is also worth mentioning that both the symmetrical star patch and partial ground plane are exploited in order to compensate the bending effect.

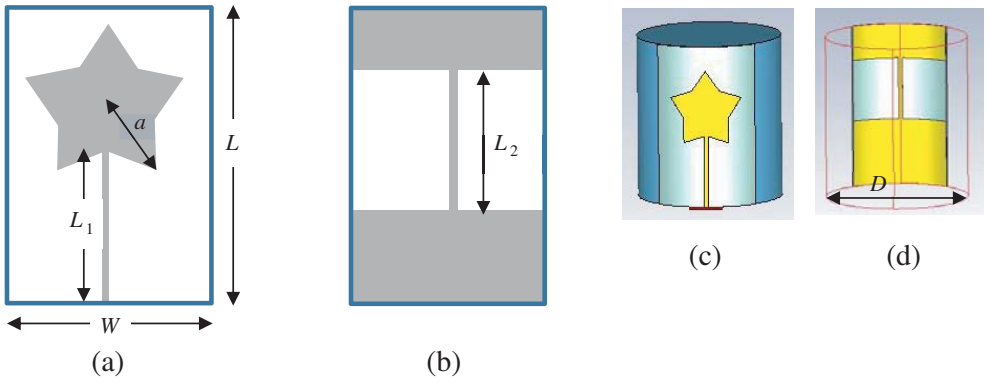

Figure 1. Geometry of the star patch wearable antenna: (a) Star patch from the top view ($W = 50$ mm; $L = 75$ mm, microstrip-line feed with the dimension of $L_1 = 34$ mm and width of 3.372 mm, (b) partial ground plane from the bottom view with $L_2 = 28.5$ mm, (c) top view of the star patch in CST MWS®software; and (d) partial ground plane is bending on a curvy structure with diameter (D).

3. RESULTS AND ANALYSIS

3.1. Reflection Coefficient

The antenna is simulated under different bending conditions in CST MWS software. Figure 2(a) shows that the simulated reflection coefficient, S_{11}, at flat condition is -26.67 dB at 2.45 GHz. It is also demonstrated that when the prototype is bent on a curvy surface with diameter, $D = 120$ mm, 90 mm,

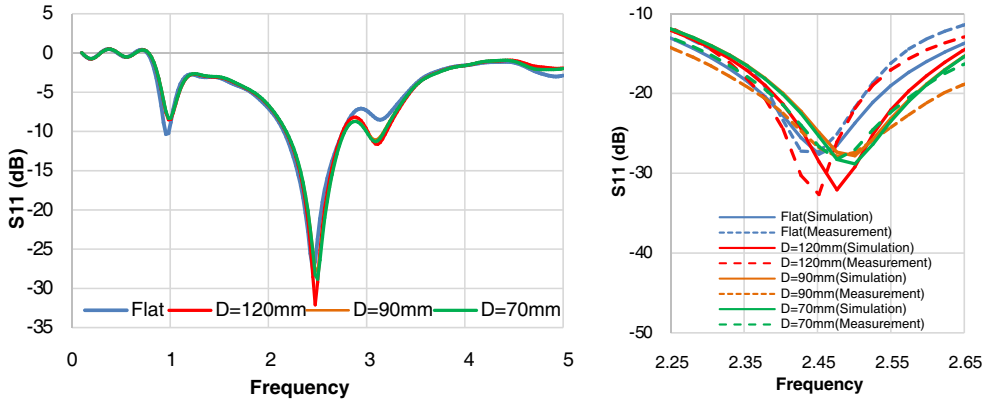

(a) (b)

Figure 2. (a) Simulated reflection coefficient of the star patch antenna under various bending conditions. (b) Comparison between simulated and measured results.

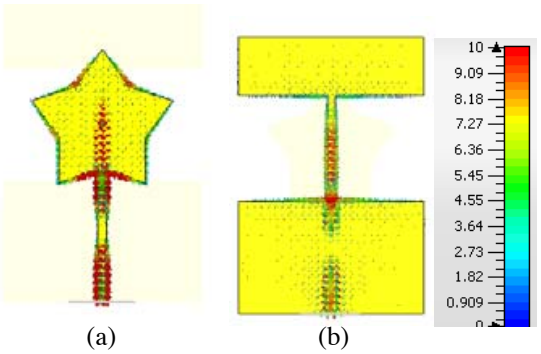

(a) (b)

Figure 3. Surface current at 2.45 GHz on (a) star patch, (b) partial ground plane.

(a) (b) (c) (d)

Figure 4. (a) Measurement setup of the star patch antenna in bending condition with various diameters, D of the plastic cylinder; (b) $D = 120$ mm, (c) $D = 90$ mm; and (d) $D = 70$ mm.

and 70 mm, S_{11} is slightly improved, and the value approaches -30 dB. Therefore, in order to explain this phenomenon, surface current distributions and electric field intensity have been generated from the simulations in CST MWS software as shown in Figure 3. From the figure, it can be clearly seen that the maximum surface current occurs at the edges of the star patch when the electric field is excited in the vertical direction. On the other hand, the maximum surface current occurs along the middle line which is parallel to the star patch antenna, on the partial ground plane. The verification of the simulated S_{11} is performed by connecting the radiating patch to the Rohde & Schwarz ZVB14 vector network analyzer as illustrated in Figure 4. In the measurements, the setup of antenna in flat condition

is carried out in two conditions; firstly, the antenna is measured alone, and secondly, the antenna is placed on a plastic flat surface. It has been observed that the measured results are relatively similar, and therefore, it can be concluded that the plastic bottle does not introduce any additional intolerances to the structure. At $D = 120$ mm, the simulated resonant frequency is shifted to 25 MHz higher from the resonant frequency obtained in the flat condition. Meanwhile, at $D = 90$ mm and 70 mm, the resonant frequency is shifted to 50 MHz higher. However, the -10 dB bandwidth of the star patch antenna is approximately 600 MHz, which overcomes the shift in the resonant frequency caused by the bending effect. For verification of simulated antenna performance at various bending conditions, the fabricated antenna is attached to a plastic cylinder with the specified diameter, D. The measured S_{11} demonstrate a strong agreement as the resonant frequency is not shifted more that 1% from the simulated results as illustrated in Figure 2(b).

3.2. Radiation Pattern

Far-field radiation patterns of the star patch antenna have been measured in an anechoic chamber as can be seen in Figure 5. The comparison between the simulated and measured radiation patterns in the E-plane (yz-cut) and H-plane (xz-cut) are shown in Table 1. The antenna-under-test (AUT) is placed on the ETS-Lindgren 2090 positioner and aligned to the horn antenna with adjustable polarization. From the table, it is shown that the antenna has an omnidirectional pattern at 2.45 GHz. In flat condition, the simulated maximum directivity in the H-plane is 129.55 dBuV/m, and this value is reduced to 128.2 dBuV/m at $D = 90$ mm and 70 mm. For E-plane, in flat condition, the directivity of the main lobe is 138.3 dBuV/m and is reduced to 136.9 dBuV/m at $D = 90$ mm) and 130.6 dBuV/m at $D = 70$ mm. The measured directivity shows a good agreement with the simulated results. It is also observed that the antenna radiation patterns are relatively insensitive to bending conditions at $D = 90$ mm and 70 mm. It is observed from the simulation results that the SAR effect is slightly higher than the international standard, and this is expected as the partial ground plane allows the electric field to penetrate into the body tissues. For clarification, the details of SAR effects to the human body are not discussed in this paper, and it is also worth to highlight that the SAR limit may be improved by using EBG substrate [12].

Figure 5. Radiation pattern measurement setup in an anechoic chamber; (a) H-plane (xz-cut). (b) E-plane (yz-cut). (c) Gain measurement setup; calibration of VNA using two horn antennas and AUT later replaced with star patch.

3.3. Gain

The gain transformation method technique is employed to measure the antenna gain in the anechoic chamber. Two horn antennas are set up to serve as the gain reference. Next, one horn antenna is replaced with the star patch antenna as the antenna-under-test (AUT) as can be seen in Figure 5(c). Figure 6 shows the simulated and measured gains of the star patch antenna under various bending conditions. The antenna has a gain of 3.404 dB in flat condition, 3.749 dB at $D = 90$ mm and 3.814 dB at $D = 70$ mm at the operating frequency of 2.45 GHz. It is observed that the gain of the antenna slightly increases when the bending curves are increased in diameter, which can be attributed to higher surface current concentration. The measured gain is extracted by using a classic gain-transfer method

by assuming a uniform plane wave incident over the aperture of horn antenna as well as the AUT [13]. Discrepancies in the simulated and measured gains of the AUT can be significant, especially when there is a large difference in aperture dimension between the AUT and standard-gain horn. In this case, the size of AUT is 1/10 of the standard-gain horn and thus, producing differences in gain from 0.6 to 1.6 dB at the resonant frequency of the antenna. The surrounding environment may also contribute to the discrepancies, such as the mineral water bottle used as a platform for bending investigation, which is not modeled in the simulation.

Table 1. Simulated (solid line) and measured (dotted-line) radiation patterns under various bending conditions.

Condition	*H*-plane (*xz*-cut)	*E*-plane (*yz*-cut)
Flat	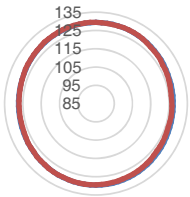	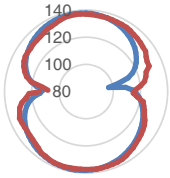
D =90	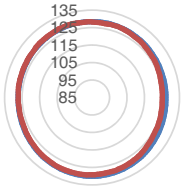	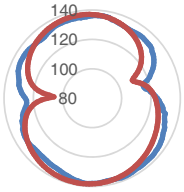
D =70	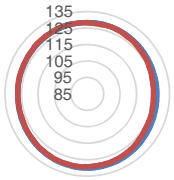	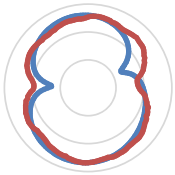

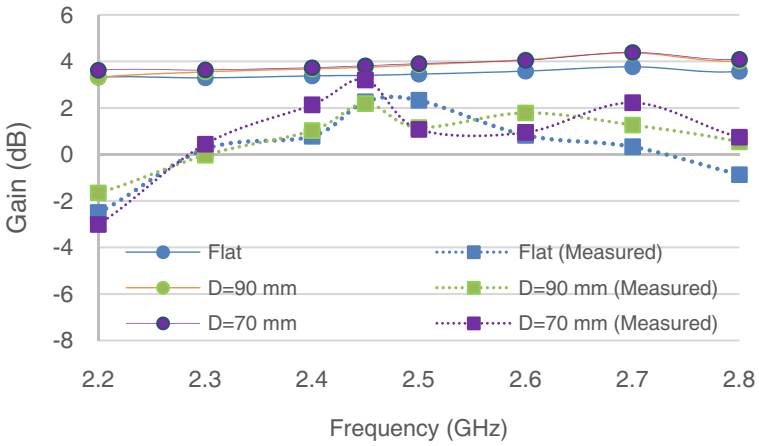

Figure 6. Simulated and measured gain of the star patch antenna under various bending conditions.

4. CONCLUSION

In this work, a star patch antenna on Kapton Polyimide Film is proposed which operates at 2.45 GHz. The antenna is tested under various bending conditions, and it is observed that the performance of the antenna is not compromised. Therefore, the antenna in this work can serve as an alternative candidate for wearable devices. In future work, the antenna will be integrated into a transceiver platform and will be tested in the actual indoor and outdoor environment to observe the actual performance.

ACKNOWLEDGMENT

This work is supported as part of the Fundamental Research Grant Scheme (FRGS) [Vot 1629] provided by the Ministry of Education (MOE) Malaysia and Postgraduate Research Grant (GPPS) [Vot H026].

REFERENCES

1. MohdRais, N. H., P. J. Soh, M. F. A. Malek, and G. A. E. Vandenbosch, "Dual-band suspended-plate wearable textile antenna," *IEEE Antennas and Wireless Propagation Letters*, Vol. 12, 583–586, 2013.
2. Whittow, W. G., et al., "Inkjet-printed microstrip patch antennas realized on textile for wearable applications," *IEEE Antennas and Wireless Propagation Letters*, Vol. 13, 71–74, 2014.
3. Chen, S. J. and C. Fumeaux, "Wearable antennas based on graphite paper and conductive polymer," *12th European Conference on Antennas and Propagation (EuCAP 2018)*, 1–4, London, 2018.
4. Sabban, A., "Small wearable antennas for wireless communication and medical systems," *2018 IEEE Radio and Wireless Symposium (RWS)*, 161–164, Anaheim, CA, 2018.
5. Li, W., W. Chung, F. Hsiao, T. Kao, and M. Huang, "Conformal integrated multi-layer thin-film antenna by novel LITA technologies for smartwatch wearable device applications," *2016 International Symposium on Antennas and Propagation (ISAP)*, 22–23, Okinawa, 2016.
6. Poonkuzhali, R., Z. C. Alex, and T. N. Balakrishnan, "Miniaturized wearable fractal antenna for military applications at VHF band," *Progress In Electromagnetics Research C*, Vol. 62, 179–190, 2016.
7. Seman, F. C., C. Manoharen, Z. Z. Abidin, and F. A. Poad, "Performance evaluation and implementation of semi-flexible dipole antenna for Internet of Things applications," *2017 IEEE Asia Pacific Microwave Conference (APMC)*, 158–161, Kuala Lumpar, 2017.
8. Ahmed, S., F. A. Tahir, A. Shamim, and H. M. Cheema, "A compact kapton-based inkjet-printed multiband antenna for flexible wireless devices," *IEEE Antennas and Wireless Propagation Letters*, Vol. 14, 1802–1805, 2015.
9. Khaleel, H. R., H. M. Al-Rizzo, D. G. Rucker, and S. Mohan, "A compact polyimide-based UWB antenna for flexible electronics," *IEEE Antennas and Wireless Propagation Letters*, Vol. 11, 564–567, 2012.
10. Yuningtias, E., R. Yuwono, E. B. Purnomowati, G. Dhuha, and F. Ramadhan, "Star patch microstrip antenna for UWB," *The 14th International Conference on Quality in Research, (QiR)*, 2015.
11. Jilani, S. F., H. Ur-Rahman, and M. N. Iqbal, "Novel star-shaped fractal design of rectangular patch antenna for improved gain and bandwidth," *2013 IEEE Antennas and Propagation Society International Symposium (APSURSI)*, 1486–1487, Orlando, FL, 2013.
12. Ashyap, A. Y. I., Z. Z. Abidin, S. H. Dahlan, H. A. Majid, and F. C. Seman, "A compact wearable antenna using EBG for smart-watch applications," *2018 Asia-Pacific Microwave Conference (APMC)*, 1477–1479, Kyoto, 2018.
13. Mayhew-Ridgers, G., P. A. van Jaarsveld, J. W. Odendaal, and J. Joubert, "Accurate gain measurements for large antennas using modified gain-transfer method," *IEEE Antennas and Wireless Propagation Letters*, Vol. 13, 369–371, 2014.